Pollutant dispersion in a large indoor space

Part 2 - Computational Fluid Dynamics (CFD) predictions and comparison with a scale model experiment for isothermal flow

Elizabeth U. Finlayson, Ashok J. Gadgil, Tracy L. Thatcher*, and Richard G. Sextro

Indoor Environment Program

Lawrence Berkeley National Laboratory

1 Cyclotron Road MS 90R3058

Berkeley CA 94720

* corresponding author: tel: 510-486-5215

FAX: 510-486-6658

e-mail: tlthatcher@lbl.gov

Abstract

This paper reports on an investigation of the adequacy of Computational fluid dynamics (CFD), using a standard Reynolds Averaged Navier Stokes (RANS) model, for predicting dispersion of neutrally buoyant gas in a large indoor space. We used CFD to predict pollutant (dye) concentration profiles in a water filled scale model of an atrium with a continuous pollutant source. Predictions from the RANS formulation are comparable to an ensemble average of independent identical experiments. Model results were compared to pollutant concentration data in a horizontal plane from experiments in a scale model atrium. Predictions were made for steady-state (fully developed) and transient (developing) pollutant concentrations. Agreement between CFD predictions and ensemble averaged experimental measurements is quantified using the ratios of CFD-predicted and experimentally measured dye concentration at a large number of points in the measurement plane. Agreement is considered good if these ratios fall between 0.5 and 2.0 at all points in the plane. The standard k-epsilon two equation turbulence model obtains this level of agreement and predicts pollutant arrival time to the measurement plane within a few seconds. These results suggest that this modeling approach is adequate for predicting isothermal pollutant transport in a large room with simple geometry.

Keywords: CFD, Experimental verification, RANS model, Indoor pollutant dispersion

1. Introduction

The transient transport and dispersion of airborne pollutants in large indoor spaces (such as atriums, auditoriums, theaters, airport lounges, and subway stations) is an area of continued scientific and practical interest. An improved understanding of such pollutant transport will facilitate the assessment of the risk to occupants from a release of an airborne toxic pollutant in the space, and help identify and evaluate ways to reduce occupant exposures in the event of such release. One example application would be saving occupants during an acutely toxic release of long duration in a large indoor public place. Another would be achieving improved isolation of non-smoking sections of large spaces from the cigarette smoke emanating from smoking sections.

Scientific research on air flows and pollutant transport in large interior spaces is an emerging field. The literature is sparse compared to that on pollutant transport processes in atmospheric boundary layers. While many experimental and computational studies exist for air flow and temperature distribution in indoor spaces, most have investigated occupant comfort (which depends on local air velocity, humidity and temperature), rather than pollutant transport.

A common method for investigating indoor pollutant transport is to assume that the release is instantaneously and uniformly mixed throughout the space. This assumption, while useful and acceptable for estimating exposures in many circumstances, is a poor approximation for acute and short-term exposures in large indoor spaces. It is also an inadequate approximation

for situations like the one investigated here with a long term continuous release in which the space never achieves a fully mixed state.

For point pulse release in an indoor space with negligible air exchange with outside, Baughman et al. (1994) introduced the concept of mixing time. Baughman et al (1994) and Drescher et al. (1995) measured mixing time for pulse release of point pollutants in a small, ~31 m^3 room under various conditions. Baughman investigated mixing driven by purely natural convection , using a tracer to simulate the smoldering of a cigarette for ten minutes. Drescher et al (1995) measured mixing times in a single room under conditions approaching purely mechanical mixing, and correlated it with mechanical power supplied to the room air. Drescher et al. found the mixing time to vary between 2 and 42 minutes depending on the mechanical power supplied to the room air. For exposures over time scales much longer than the mixing time, the instantaneous perfect mixing approximation might be acceptable. For time scales comparable to or shorter than the mixing times, something more precise than the perfect mixing approximation is warranted. For continuous releases, the mixing time approximation may not be useful.

A few researchers have tried to improve upon the instantaneous perfect mixing assumption. Rassouli and Williams (1995) applied an analytic model to analyze indoor gas dispersion. However, most of the limited published work on this topic relies on computational fluid dynamics (CFD) models. Murakami et al. (1994) compared predictions from various turbulence models for a non-isothermal jet in a room. Emmerich (1997) reviewed the use of CFD as a tool to analyze indoor air quality. A purely numerical study of the full scale

experimental atrium facility was performed by Grinstein and Boris (2001). This study investigated pollutant transport in an isothermal room as well as a room with differentially heated surfaces, using a single realization of an LES type of numerical model. There are only a few publications comparing CFD predictions of room mixing with experimental measurements. Shimada et al (1996) compared experiments and CFD predictions for aerosol particle concentrations in industrial clean rooms. Mizuno and Warfield (1992) compared experimental measurements of air flows and particle concentrations with CFD predictions for airplane cabins. However, both these papers addressed specialized spaces and ventilation configurations unlike those commonly encountered in large indoor spaces. Chen (1997) and Chen and Chao (1996) compared experimental data for aerosol concentrations and air flow in a room with a heat source with predictions made using two different turbulence models. Furtow et al. (1996) reported measurements of air quality in imperfectly mixed rooms and modeled it using a known air flow field. More recently, Gadgil et al. (2000) obtained CFD predictions for room mixing time using a method similar to the one described in this paper and compared them to the published experimental results obtained earlier. Their predictions were in good agreement with the experimental data. A larger bibliography of relevant published literature, including purely experimental and purely computational work, is given in Gadgil et al. (2000).

Most of the published research comparing pollutant transport measurements with CFD predictions shares the shortcoming of sparse spatial and temporal sampling of the pollutant concentration. This results in a limited number of data points that can be checked against CFD predictions. Furthermore, owing to the poor time resolution of most measurement

methods, it is rare to find comparisons of CFD predictions with experimental measurements of transient pollutant dispersion in rooms.

The lack of high quality, spatially and temporally resolved, experimental data makes robust comparisons between prediction and measurement difficult. Remote and non-intrusive methods to obtain tracer gas concentration maps in indoor spaces with high spatial and temporal resolution (on the order of 1 meter, and 10 seconds, respectively) are just beginning to reach maturity (Price et al. 2001, Fischer et al. 2001). Comparisons are even more problematic when developing flow or concentration conditions are explored. The experimental study of transient dispersion under turbulent flow requires a large number of replicates to obtain statistically sound estimates of ensemble averages.

The broad goal of this paper is to evaluate the adequacy of the most common of the Reynolds Averaged Navier Stokes (RANS) turbulence models, the k-epsilon (k-e) model, for making pollutant dispersion predictions in large indoor spaces. A specific goal of our work is to compare CFD predictions with our recent experimental data on pollutant dispersion with high spatial and temporal resolution in a water-filled scale model of an atrium (Thatcher et al. 2003). Standard k-e models generally give acceptable engineering predictions in bulk flows that are not critically dependent on interaction with surfaces. Thus, our expectation is that the standard k-e model might prove adequate for predicting transient and steady state dye dispersion in the water tank scale model of the indoor space. Exposure analysis literature (e.g., McBride et al. 2000, Maskarinec et al. 2000,) suggests that predictions accurate to better than a factor of 2 would be a significant advance over the current state of the art in estimating

indoor exposures from point source pollutants. The validity of this value for the figure of merit is strengthened by considering the amount of variability in the pollutant concentration at a given point in space for a continuous release in a fully developed flow. As can be expected from the nature of turbulent dispersion, even after fully developed conditions have been reached in the experimental model atrium there are significant fluctuations in concentration in the measurement plane. Figure 1 shows how the pollutant concentrations at various points in space compare for two single realizations of the fully developed flow. The dotted line shows a one to one correspondence while the solid lines indicate a factor-of-two agreement. Almost all of the data is captured within the factor-of-two lines. A full discussion of comparison of models of phenomena with a high degree of variability is beyond the scope of this paper, but interested readers can find a thorough discussion of this topic in Morgan and Henrion (1990).

Note that for an indoor space continuously ventilated with 100% fresh air, a steady pollutant release from a point source will never lead to a fully mixed condition. Even when the velocities and concentrations are fully developed (i.e., steady state), large spatial differences in concentrations will persist. In particular, the concentration near the fresh air inlets will be close to zero, that near the pollutant source will be extremely high, and that at the exhaust from the room will equal the ratio of the rates of pollutant emission and ventilation. Again, because of the turbulent nature of the flow, these spatial differences will fluctuate with time.

The benefits of experimentally verified computational models of air flow and pollutant transport are well understood. Within their domain of applicability, such models offer the only practical means to explore pollutant dispersion in occupied indoor spaces across a wide

range of parameters. The computational approach also allows effective exploration of alternative methods for pollutant containment (air curtains, alterations in ventilation inlet and outlet positions and flow rates) that would be prohibitively expensive, time consuming, or simply impossible if based solely on experimental investigation.

2. Problem Definition and Experimental Set-up

With the broad goals described above, the specific problem addressed here is that of pollutant dispersion in the breathing plane of a large isothermal mechanically ventilated atrium following the onset of a continuous pollutant release at one location on the floor. Owing to the stochastic nature of turbulence, the exact details of pollutant dispersion will differ from any single incident of pollutant release to the next, even under identical ventilation and boundary conditions. Even under fully developed conditions with stable statistics (i.e. stationary turbulence), the concentration field fluctuates in the measurement plane. A more complete discussion of the nature of turbulent flow can be found in Tennekes and Lumley (1987).

RANS turbulence models predict ensemble mean values (equivalent to averaging a large number of identical releases). The spatial and temporal fluctuations in the pollutant concentration field and hence local instantaneous exposures can not be captured by this method. However, due to the many unknowns in the problem (source location, occupant movement, variability in HVAC conditions) statistical predictions are the appropriate level of comparison. Therefore, strategies to protect occupants must be based only on large predicted

differences (e.g., of the order of 10 or 100) in concentrations and exposures. This also suggests that for assessing the suitability of a modeling approach as a guide to action, an agreement of the predicted mean values with the ensemble average of data from repeated experiments must be good, but need not be exact, since only large differences will be significant and useful for planning strategies for occupant protection.

In this paper, we focus on the comparison of results from the water-filled scale model of an atrium, and the corresponding CFD predictions. A schematic of the experimental configuration is shown in Figure 2. The 30:1 scale model used water as the working fluid. The top of the scale model was a free surface (unlike the full-size atrium which has a ceiling). Therefore, for this work we simulated the boundary conditions of the scale model, not the full-size atrium, with the CFD code. Thatcher, et al. (2003) provides a detailed description of the water tank, experimental methods, and the applicability of scale models. Based on a volumetric flow rate of one water tank volume per minute, the time scale of the tank is 15:1. This means that 1 second in the water tank is equivalent to 15 seconds in the full scale room. The impact that the scaling has on representation of the turbulent characteristics of the flow in the scale model as opposed to the full scale room are also discussed in Thatcher et al (2003).

During the experiment, dye-free water flowed into the water tank with no recirculation. A continuous pollutant release was simulated using a neutrally buoyant dye solution introduced into the tank just above the floor in the position shown in Figure 2. A mixture of dye and water exited the tank through an overflow weir. This water was not recirculated during the experiments, thus simulating a once-through ventilation system. The measurement plane was

3mm thick and centered 6 cm from the floor. A video camera recorded the concentration in the measurement plane. Images from the camera were digitized at two resolution levels: high resolution still images captured at 1 frame per second and a lower resolution video captured at 5 frames per second.

For each experimental run, the flow field was established prior to beginning dye injection, starting at least 3 minutes before the dye injection was initiated. The flow rate was such that in one minute, water with volume equal to the tank volume entered the tank. Thus 3 minutes allowed for three tank changes. Dye concentrations in the measurement plane were recorded with the video camera from before the start of the dye injection. Since each run represents only one realization of a highly variable and stochastic process, capturing the statistical variability of the developing flow required multiple runs for a given set of flow conditions. In these experiments, we typically captured about 20 replicate runs for both 5 frame per second lower resolution video and 1 frame per second higher resolution still images. Measurements for each of these realizations contained approximately 1000 frames.

For experiments with fully developed concentration profiles, dye injection was initiated 5 minutes prior to beginning image collection. Then, one image was collected every 3 seconds for 50 minutes (1000 images). The "average concentration" images show the average value at each pixel for a given set of data. Comparisons among the results from replicate sets of images showed that 1000 images provided a sufficient number of independent profiles to characterize the spatial variations in the average concentration and fluctuation intensity accurately.

3. Computational Fluid Dynamics Method

3.1 Computational Mesh and Boundary Conditions.

Plan and elevation views of the computational mesh for the scale model atrium are shown in Figure 3. The mesh has a resolution of 0.3 cm in the core. In the regions closer than 0.3 cm to any wall, the resolution in the direction normal to the wall increases to 0.06 cm. This is roughly equivalent to a 10 cm mesh size in the core and a 2 cm resolution near the wall in the full scale (30 times larger) atrium. The mesh in the core volume region, near the cut corner of the room, where the flow enters the scale model, is made to line up with the known flow direction of the jets to minimize numerical diffusion. We used a commercial computer CFD code for this calculation which can handle a nonrectangular hexahedral mesh with local mesh refinements, shown in Fig. 3A. Because the walls of the water tank are straight, the mesh could be extended vertically throughout the computational region. The mesh has 900,000 nodes.

We assumed that the volume flow rate (60 water changes per hour) enters equally partitioned among the 5 rectangular openings. The assumption that the flow was the same for each of the openings in the experimental setup was supported with our observations of the flow pattern of the small air bubbles entering the tank with the inlet flow. In order to test this computationally, the flow out of the 5 rectangular openings was varied linearly, with low flow at the top opening (20 cm/sec), average flow in the middle (22 cm/sec) and high flow at the

bottom (24 cm/sec), while keeping the total flow rate the same. Varying the distribution of the inlet flow in this manner had a negligible effect on the predicted flow field in the plane of observation, and so the equal partition distribution was used for the rest of the calculations.

We assume flat velocity profiles across each of the openings for the model boundary conditions. The actual velocity profile across the openings was not measured in the experiments, but is not expected to be uniform due to viscous shearing at the edges of the openings. However, using computational sensitivity studies, we determined that the simulation results in the plane of observation are insensitive to the details of the velocity profile. The top surface of water, which is open in the experimental tank, is modeled as a full-slip boundary condition; any surface tension effects are ignored. The remaining solid boundaries are modeled as non-slip surfaces. The dye source is modeled as a cube with surface area approximating that of the spherical source used in the experiment.

The volumes of the computational mesh and experimental scale model do not match exactly. A small error was made in building the mesh which resulted in the external dimension of the water tank matching the internal dimensions of the mesh volume. Throughout this discussion we assume that this discrepancy of 6 mm linear dimension out of 230 mm on the shortest side (about 2.5 %) is negligible.

3.2 Simulation Approach

We used a commercial CFD code developed by Computational Dynamics Limited (1999) to solve the governing equations. The selection process for the commercial code is described in Gadgil et al. (1999). Our solution approach was to first obtain the steady state velocity field for the water flow. Then using this velocity field as the fixed background, we solved the time dependent transport equation for the neutrally buoyant dye being released in the water.

For modeling turbulence, we used the constant property high Reynolds number k-epsilon model with standard wall functions. Along with the turbulence model, the steady state Navier-Stokes equations, using the Einstein summation convention, take the following dimensional form (e.g. Townsend 1976):

$$\frac{\partial U_j}{\partial x_j} = 0 \tag{2}$$

$$U_j \frac{\partial U_i}{\partial x_j} = -\frac{1}{\rho}\frac{\partial p}{\partial x_i} + \frac{\partial}{\partial x_j}\left(\nu \frac{\partial U_i}{\partial x_j}\right) + \frac{2}{3}\frac{\partial k}{\partial x_i} \tag{3}$$

$$U_j \frac{\partial k}{\partial x_j} = \frac{\partial}{\partial x_j}\left(\nu \frac{\partial k}{\partial x_j}\right) + \nu_{turb}\left(\frac{\partial U_i}{\partial x_j} + \frac{\partial U_j}{\partial x_i}\right)\frac{\partial U_i}{\partial x_j} - \varepsilon \tag{4}$$

$$U_j \frac{\partial \varepsilon}{\partial x_j} = \frac{\partial}{\partial x_j}\left(\frac{\nu}{1.22}\frac{\partial \varepsilon}{\partial x_j}\right) + \frac{\varepsilon}{k}\left[1.44\left(\frac{\partial U_i}{\partial x_j} + \frac{\partial U_j}{\partial x_i}\right)\frac{\partial U_i}{\partial x_j}\right] - 1.92\frac{\varepsilon^2}{k} \tag{5}$$

$$\frac{\partial C}{\partial t} + U_j \frac{\partial C}{\partial x_j} = \frac{\partial}{\partial x_j}\left(D_{molec} + \frac{\nu_{turb}}{\sigma_m}\right)\frac{\partial C}{\partial x_j} \tag{6}$$

$$\nu = \nu_{turb} + \nu_{molec} \quad (8)$$

where

P is the pressure

U_i are the velocity components,

x_i are rectilinear orthogonal coordinates

k is the turbulent kinetic energy

ε is the dissipation rate of k

C is the dye concentration

ν_{molec} is the molecular kinematic viscosity

ν_{turb} Nu-turb is the turbulent kinematic viscosity : $\nu_{turb} = 0.09k^2\varepsilon^{-1}$

D_{molec} is the molecular diffusivity of water in water.

For our simulations, we assigned the turbulent Schmidt number a value of 0.9 within 6 cm of the wall and 0.5 in the core flow based on advice from our colleague David Wilson (2000). We also ran cases using a turbulent Schmidt number of 0.9 and 0.5 throughout. The effect of these variations was not significant. Spatially, we used an implementation of the second order differencing scheme based on a Godunov method modified for incompressible flow (Van Leer 1979, Asproulis 1994). The advantage of this scheme is that it suppresses numerical diffusion without causing instability. Its disadvantage is that it slows down the computations compared to the commonly used Patankar-Spalding differencing scheme. Our exploratory computations showed that predictions made with the Patankar-Spalding differencing scheme

were too dispersive and resulted in predictions which did not agree as well with the experiments as the results discussed in the paper. A first order implicit time differencing scheme was used for the solution of the mass transport equation.

Velocity computations were terminated when the cumulative normalized residual of each of the equations dropped below 1.0e-3. The pollutant concentration calculations were terminated when the cumulative normalized residual on the mass transport equation dropped below 1.0 e-4. All CFD predictions were tested to ensure spatial grid independence. For the transient calculations, we also tested and confirmed time-step independence of the predictions.

All computations were performed on an SGI Origin 2000 machine; using one processor the computations took 72 hours to obtain the steady velocity field. This flow field formed the basis for the dye dispersion simulations. Steady-state concentration field predictions of the fully developed dye dispersion required 0.5 hours. Transient concentration field predictions to describe the onset and development of the dye dispersion took 36 hours.

4. Results

We present the comparison of computational predictions with experimental results in two sections. The first section describes the fully developed concentration field and the second describes the transient, developing concentration field.

4.1 Fully developed flow condition:

Selected sections of the computational results for the velocity field are shown in Figure 4. Fig. 4A shows a vertical plane perpendicular to the wall containing the inlets. The five inlet jets merge near the central region of the tank, and reach the opposite wall where they split, with part of the flow downward and part upward. This agrees with the qualitative behavior of the jets observed experimentally, by illuminating and visually tracking the extremely fine air bubbles entrained in the inlet water. Fig. 4B1 shows the velocity profile in a horizontal plane located at the middle inlet jet (as indicated in Figure 3A). The velocity in this section is typical of most of the volume. It divides into two large counter-rotating vortices with vertical axes, separated by the inlet flow.

Figure 4B2 shows the velocity field in the measurement plane. The measurement plane is located well below the lowest inlet jet, as indicated in Figure 3B. There is a counter clockwise flow in this plane that spirals upwards in the lower left corner. The flow from the jets enters the breathing plane near the lower right corner. These flow characteristics are also consistent with qualitative observation of the flow in the experiment.

A comparison between the experimental data and the computation predictions for the fully developed dye concentration is shown in Fig. 5 for the measurement plane. Significant fluctuations persist even when the pollutant concentration is considered fully developed or computationally has reached a steady state. For this figure, the experimental data are an ensemble average obtained by combining 1000 images. The number of images required was

determined by examining both the mean concentration and fluctuation intensity of the fully developed concentration profiles and increasing the number of images in the averaging process till these two measures reached stable values (Thatcher 2003). The fluctuation intensity equals the standard deviation of the local value of the concentration divided by the local mean concentration. Comparisons between the results from different experiments showed that 1000 images provided a sufficient number of independent profiles to obtain a meaningful average concentration profile. The agreement between the measurements and the simulation results appears qualitatively very good. To a small extent, the dye concentration is over-predicted in regions of high concentration, and under-predicted in regions of low concentration.

The prediction and experimental result shown in Fig. 5 are quantitatively compared in Figs. 6 and 7. For these comparisons, the computational prediction was evaluated at locations in the measurement plane corresponding to locations of each of the pixels in the digital photographs obtained in the experiment. The local concentration, for both the experimental data and the computational results, was divided by the value of the fully developed concentration from the experiment. A grid array of 1.3 x 1.3 cm squares (10 by 12 pixels in the experimental data, corresponding to a 39 cm by 39 cm square in the breathing plane for the full scale atrium) was superimposed on the measurement plane, resulting in 456 regions.

The normalized concentration values for each of these regions from the experiment and the CFD calculation were plotted against each other to obtain Fig. 6. A perfect agreement at all the spatial regions would have resulted in all the data-points lying on a single line of unit

slope. The best linear fit to the data, forced through the origin, has slope 1.1 and R-squared value of 0.66. The computational predictions are centered correctly, with only a 4% difference in the average breathing plane concentrations predicted with CFD and measured in the experiment. However, the simulations somewhat under-predict the concentration in the regions of low concentrations, and somewhat over-predict the concentration in the regions of high concentrations (giving rise to the slope of larger than unity). When these 456 ratios, one for each region, are rank ordered, their cumulative distribution is shown in Figure 7. For a perfect fit, the cumulative distribution curve would be vertical line at X=1.0. From this curve the median ratio of 1.15 can be obtained. This distribution also shows that the concentration ratios of CFD predictions to experimental observations at all regions are well within a factor of 2. We conclude that the readily available two equation (k-e) turbulence model yields acceptably good results steady state predictions for fully developed concentrations in the breathing plane (and hence occupant exposures).

4.2 Transient flow conditions:

A comparison of fully developed dye dispersion predictions with experimental results tests the accuracy of the spatial dispersion simulations, but not the temporal nature of the dispersion following release. Just as it is important to evaluate model results in steady state, one must also determine the acceptability of the model for predicting transient and acute exposures to pollutants. Therefore, we now turn to a test of model predictions under transient conditions; modeling spread of the pollutant in the breathing plane after its sudden onset and comparing with experimental observations. Note that in the experiments, the dye release was

continuous throughout each test after its onset, as it was for the simulations. So, this comparison is based on the data and simulation predictions for the first few minutes of each test run.

The dye first appears in the breathing plane approximately 5 seconds after the dye is released from its source on the floor of the scale model (see Figure 2). Images from experimental results of developing dye concentration profile in the breathing plane, for various elapsed times are shown in Fig. 8. The four images show two early times (12 and 36 s after release, respectively) in addition to the dye concentration after one and three volume exchanges (60 and 180 s respectively). The experimental images are the average of images from 19 independent experiments, taken at the same elapsed time after the start of dye release.

In addition to showing the growth of the plume in the breathing plane, these images also show small areas of high concentration which are fluctuations in the concentration field. The presence of these fluctuations is an indication that 19 replicate experiments were an insufficient number to obtain a stable ensemble average in this developing flow. However, the replicates are sufficient in number to provide a reasonable sense of the time evolution of the average concentration profile. We use the average results from these 19 replicates for comparison with the CFD predictions with the understanding that though not perfect, they provide a closer approximation to the true ensemble average than does a single realization. Experience with fully developed dye dispersion experiments suggests that more than 200 independent images would be needed for obtaining stable ensemble average data. (Thatcher, 2003).

CFD simulations of the dye concentration profiles in the breathing plane for the same elapsed times as shown for the experimental data are presented in Figure 9. Compared to the experimental results which show measurable amounts of dye reaching the breathing plane in 5 seconds, the numerical results predict that the dye will be measurable at 4 seconds. This is within experimental error associated with the actual emergence of the dye from the experimental dye source. The agreement between corresponding frames in Figs 8 and 9 is qualitatively very good.

Quantitative comparisons between the predictions and experimental results at the different elapsed times were performed with the same method as used for the steady-state comparisons shown in Fig. 6. These comparisons are shown in Fig. 10. A cumulative comparison, plotting all the data points in Fig. 10 on a single plot, is shown in Fig. 11. The least square fit of this data has a slope of 0.98 and an R^2 value of 0.83. These quantitative results show that the standard two-equation (k-e) turbulence model provides adequate predictive accuracy (much better than a factor-of-2) for spatial and temporal dispersion from sudden onset of the continuous point source release.

5. Summary and conclusions

Work described in this paper addresses improved predictions of short-term and localized exposure to pollutants in indoor spaces under isothermal conditions. We describe results from a scale model of an isothermal atrium to study the dispersion of a surrogate pollutant (dye

release in water as the working fluid) in the breathing plane. We compare the dye concentration measured in the breathing plane to predictions from a standard RANS two-equation (k-e) model for both steady-state dispersion and transient dispersion after a sudden onset of a point-source release on the floor.

Our results show that when carefully implemented, the standard RANS two-equation k-e model predicts breathing plane concentrations in the transient and steady-state case experiments to substantially better than a factor-of-two. These results represent one of the first intercomparisons of experiments and simulations for both flow and contaminant dispersion within an indoor space with high spatial and temporal resolution. Complex flow patterns observed in the experiments were simulated with reasonable fidelity, providing confidence in both the capturing of the underlying physics in the commercial CFD code, and our choice of the standard RANS two-equation (k-e) turbulence model for these isothermal conditions.

The experiments and modeling work described in this work were limited to isothermal flows. Future work will need to address predictions under non-isothermal conditions in more realistic geometries such as the full scale atrium described in Gadgil (2000).

6. References

Asproulis, P.N. 1994. “High Resolution Numerical Predictions of Hypersonic Flows on Unstructured Meshes”, Ph.D. Dissertation, Imperial College, Dept. of Aeronautics, London, England.

Baughman, A. V., Gadgil, A. J. and Nazaroff, W. W., 1994, "Mixing of a point source pollutant by natural convection flow within a room." *Indoor Air **4**,* pp. 114-122.

Computational Dynamics Limited – 1999 Methodology STAR-CD Version 3.10.

Drescher, A. C., Lobascio, C., Gadgil, A. J. and Nazaroff, W. W., 1995, "Mixing of a point-source indoor pollutants by forced convection." *Indoor Air* **5**, pp. 204-214.

Chen, Q., 1997, "Computational fluid dynamics for HVAC: Successes and failures." *ASHRAE Trans.* **103(l),** pp. 178-187.

Chen, Q, Chao, N-T. 1996. Prediction of Buoyant Plume and Displacement Ventilation with Different Turbulence Models. *Proceedings of the 7th International Conference on Indoor Air Quality and Climate – Indoor Air ’96*, Vol. 1, pp 787-792.

Emmerich, S J. 1997. Use of Computational Fluid Dynamics to Analyze Indoor Air Quality Issues, NISTIR 5997. National Inst. of Standards and Technology. Gaithersburg, MD, USA. flame.cfr.nist.gov/bfrlpubs/build97/art016.html.

Fischer, M. L., Price, P. N., Thatcher, T. L., Schwalbe, C. A., Craig, M. J., Wood, E. E., Sextro, R. G., and Gadgil, A. J., “Rapid Measurement and Mapping of Tracer Gas Concentrations in a Large Indoor Space.” Atmospheric Environment, Vol. 35 (2001) pp. 2837-2844 . LBNL-45542.

Furtaw, E. J., Jr. Pandian, M. D., Nelson, D.R. and Behar, J. V., 1996, "Modeling indoor air concentrations near emission sources in imperfectly mixed rooms." J *Air & Waste Manage. Assoc.* **46**, pp. 861-868.

Gadgil, A. J., Finlayson, E. U., Hong K. H., Sextro R. G. 1999. "Commercial CFD Software Capabilities for Modeling a Pulse Release of Pollutant in a Large Indoor Space." *Proceeding of Indoor Air 99: the 8th International Conference on Indoor Air Quality and Climate.* Edinburgh August 1999.

Gadgil, A. J., Finlayson, E. U., Fischer, M. L., Price, P. N., Thatcher, T. L., Craig, M. J., Hong, K. H., Housman, J., Schwalbe, C. A., Wilson, D., Wood, J. E., and Sextro, R. G., 2000. "Pollutant Transport and Dispersion in Large Indoor Spaces: A Status Report for the Large Space Effort of the Interiors Project." Lawrence Berkeley National Laboratory report LBNL-44791. June 2000.

Gadgil, A.J., Lobscheid, C., Abadie M.O.and Finlayson E.U., Indoor Pollutant Mixing Time in an Isothermal Closed Room: An Investigation Using CFD. Lawrence Berkeley National Laboratory report LBNL-51413. September 2002. (Submitted to Atmospheric Environment).

Grinstein F.F., Boris J.P. Numerical Simulation of Unsteady Buoyant Flows in Buidings. Proceedings of 2001 ASME Fluids Engineering Division Summer Meeting. June 2001. New Orleans. LA.

Maskarinec, M.P., Jenkins, R. A., Counts, R. Wl, and Dindal, A. B. 2000, "Determination of exposure to environmental tobacco smoke in restaurant and tavern workers in one US city," Journal of Exposure Analysis and Environmental Epidemiology, Vol. 10, No. 1, pp. 36-49.

McBride, S. J., Ferro, A. R., Ott, W. R., Switzer, P., and Hildemann, L. 1999, "Investigations of the proximity effect for pollutants in the indoor environment," Journal of Exposure Analysis and Environmental Epidemiology, Vol. 9, No. 6, pp. 602-621.

Mizuno, T. and Warfield, M. J., 1992,"Development of three-dimensional thermal airflow analysis computer program and verification test." *ASHRAE Trans.* **98(2)** pp. 329-338.

Morgan, G. and Fischer, M.L. Uncertainty, A Guide to Dealing with Uncertainty in Quantitative Risk and Policy Analysis. Cambridge University Press. New York. 1990.

Murakami, S., Kato, S., Ooka, R., Comparison of Numerical Predictions of a Horizontal Nonisothermal Jet in a Room with Three Turbulence Models – k-e EVM, ASM and DSM. ASHRAE Transactions. Vol. 100 (2), pp. 697-704.

Rasouli, F. and Williams, T. A., 1995, "Application of dispersion modeling to indoor gas release scenarios." *J Air & Waste Manage. Assoc.* **45***,* pp. 191-195.

Shimada, M., Okuyarna, K., Okazaki, S., Asai, T., Matsukura, M. and Ishizu, Y., 1996, "Numerical simulation and experiment on the transport of fine particles in a ventilated room." *Aerosol Sci. & Tech.* **25***,* pp. 242-255.

Tennekes, H., and Lumley, J.L. A First Course in Turbulence. The MIT Press. Cambridge Massachusetts. (1987).

Thatcher, T. L., Wilson, D.W., Wood, E., Craig, M., and Sextro, R. G. Scale Modeling of Contaminant Dispersion Indoors. Lawrence Berkeley National Laboratory report LBNL-50248. (Submitted to Indoor Air). September 2002.

Townsend, A.A. 1976. The Structure of Turbulent Shear Flow. 2nd Edition. Cambridge University Press, Cambridge. Pg. 339.

Van Leer, B. 1979. "Towards the Ultimate Conservative Difference Scheme: A Second Order Sequel to Godunov's Mehod". Journal of Computational Physics. Vol. 32, p. 101-136

Wilson, David 2000. Personal Commication.

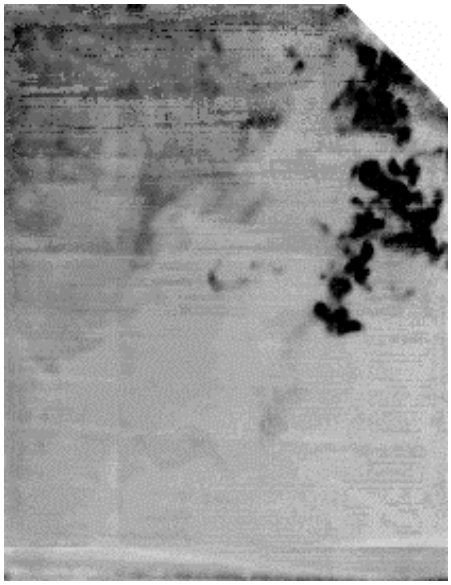

1A

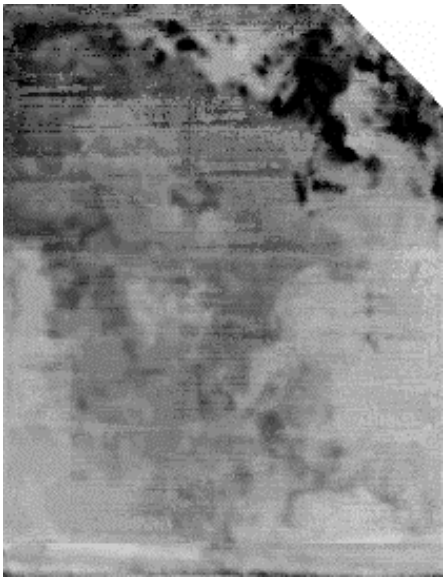

1B

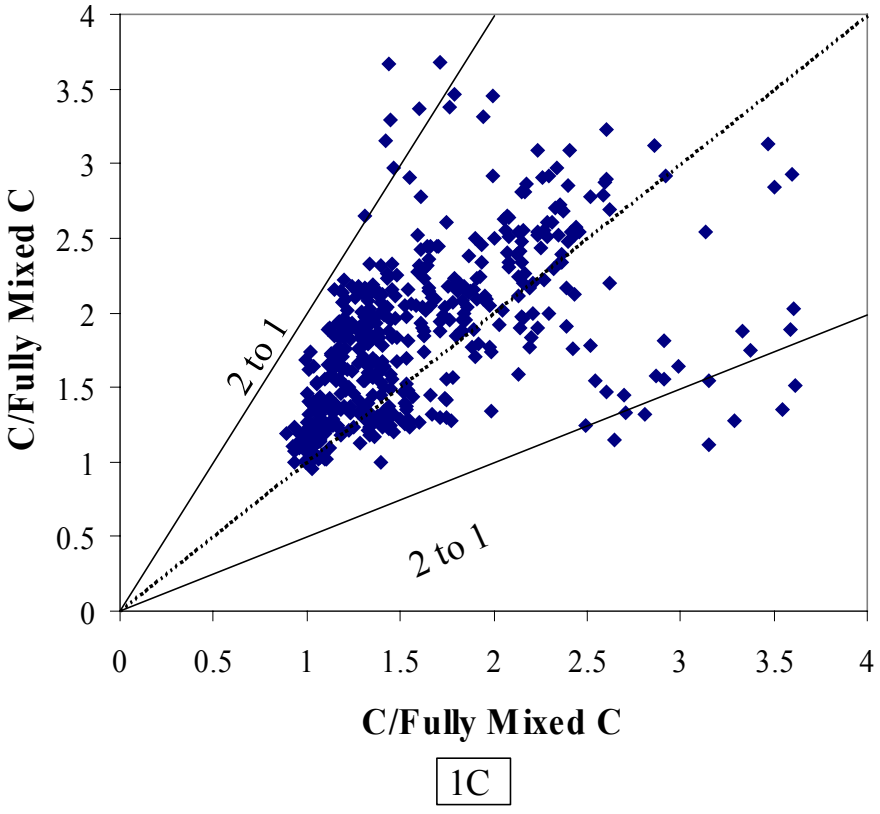

1C

Figure 1. These figures show local variations in the concentration (C) observed in the experiment. 1A and 1B are examples of the highly resolved experimental data. These are two separate realizations of the fully developed flow. 1C plots these data sets against each other. The dotted line shows a one to one fit. While the solid lines show the bound for the factor of two fit. The slope of the least square fit for this data is 1.1

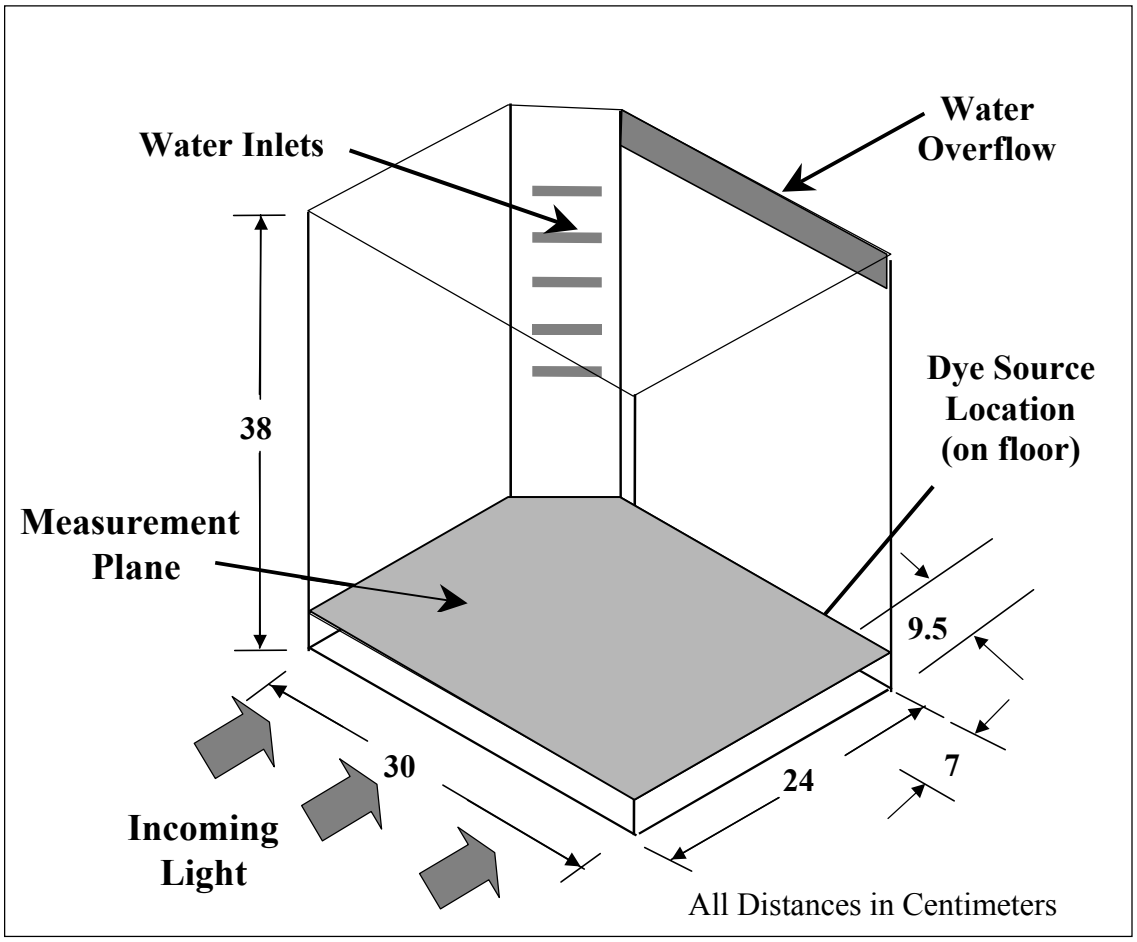

Figure 2 – Schematic of water tank used for experiments and for CFD calculations.

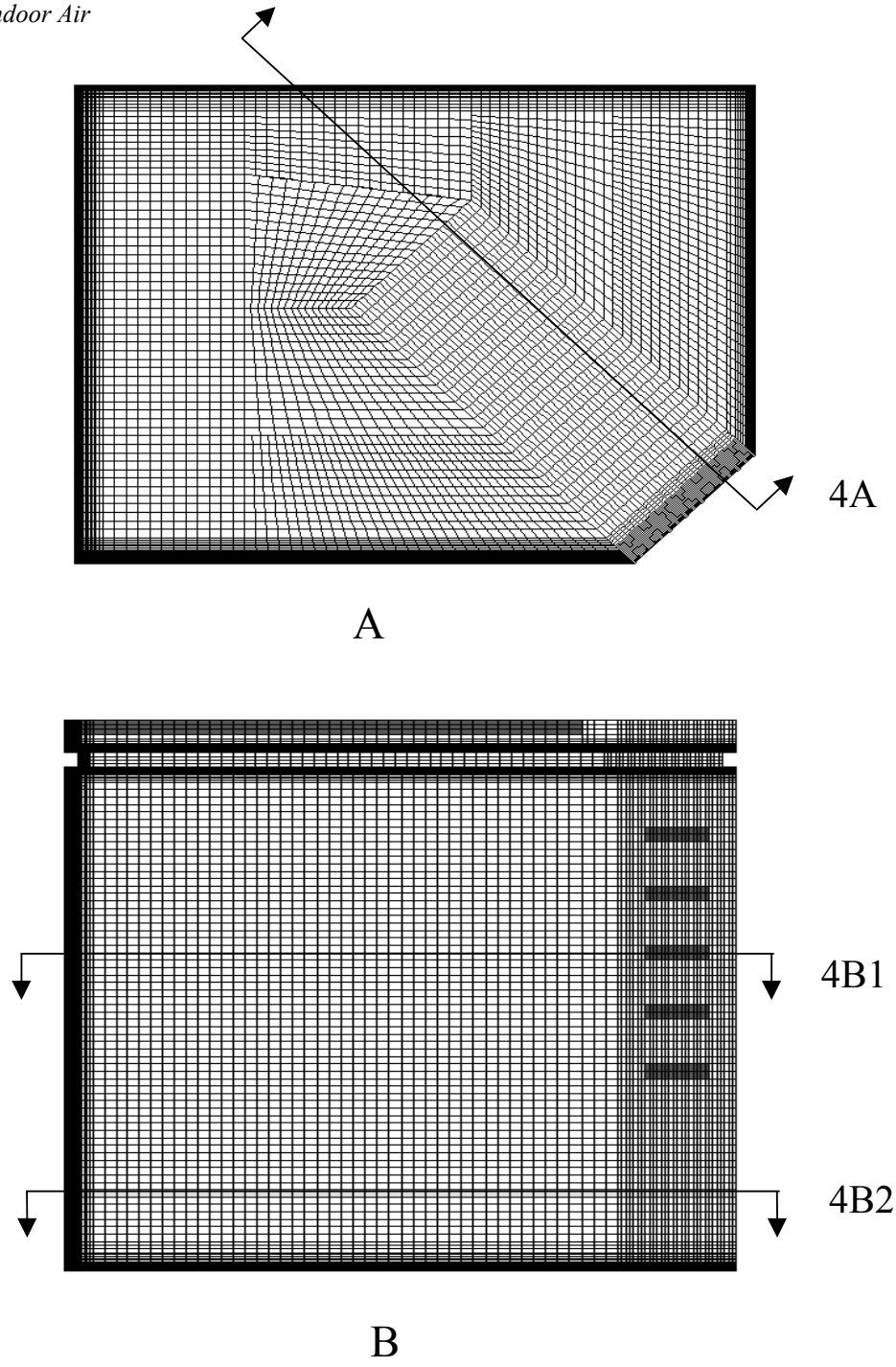

Figure 3. Computational mesh used in CFD model of the watertan
mesh is 900,000 cells. A) is an plan view of the tank, while B) is a
view of the edge of the mesh. The sections noted as 4A, 4B1 and
correspond to the respective views shown in Figure 4.

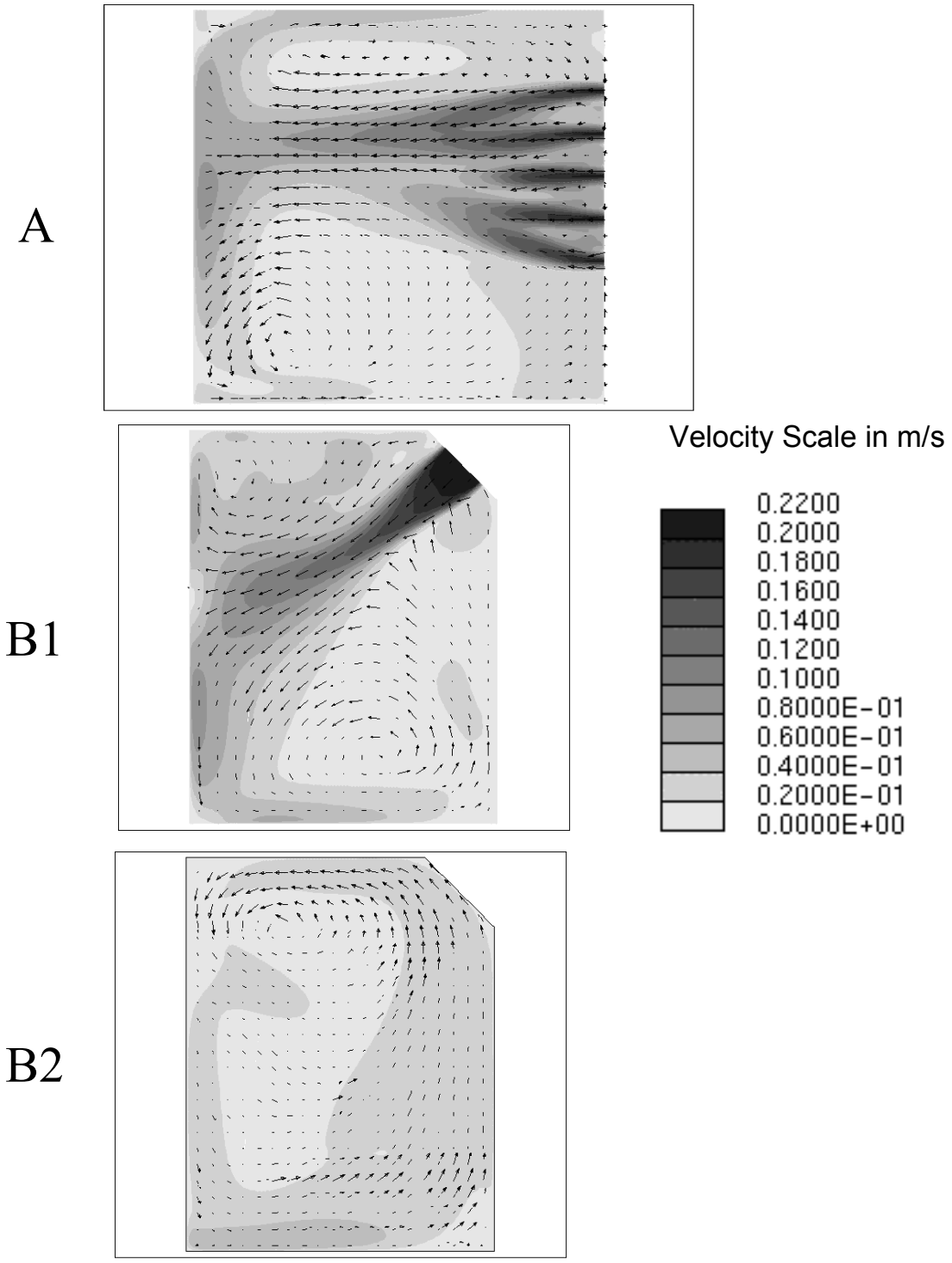

Figure 4. Velocity fields for the section views indicated in Figure 3. A) Vertical plane perpendicular to the bank of inlets; note how the jets merge together and then divide as they approach the wall of the tank. B1) Horizontal plane at the middle inlet jet; note counter rotating vortices separated by the inlet flow. B2) Horizontal plane corresponding to the measurement plane; note the single counter rotating vortex.

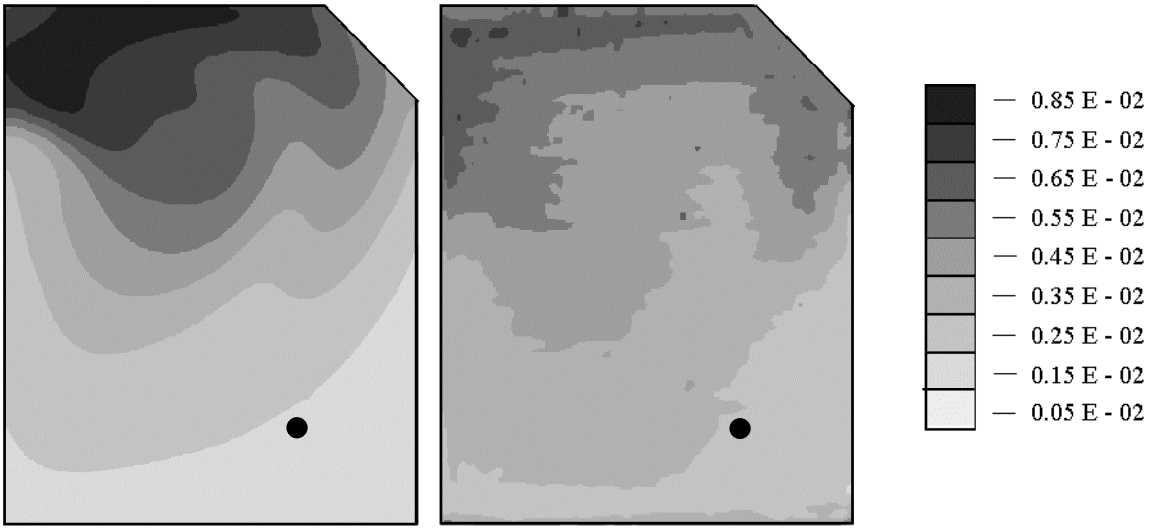

A B

Figure 5. Comparison of predicted (A) and measured (B) concentrations for fully developed flow conditions. The predictions are normalized by the mean predicted concentration from the steady-state CFD results while the measured values are normalized by experimental data for fully developed flow averaged over 3000 seconds. The maximum and minimum values for the CFD results are 0.9e-2 and 0.14e-2 respectively. The maximum and minimum values for the experimental results are 0.8e-2 and 0.17e-2. The black dot in each image indicates the location of the source, which was below the measurement plane.

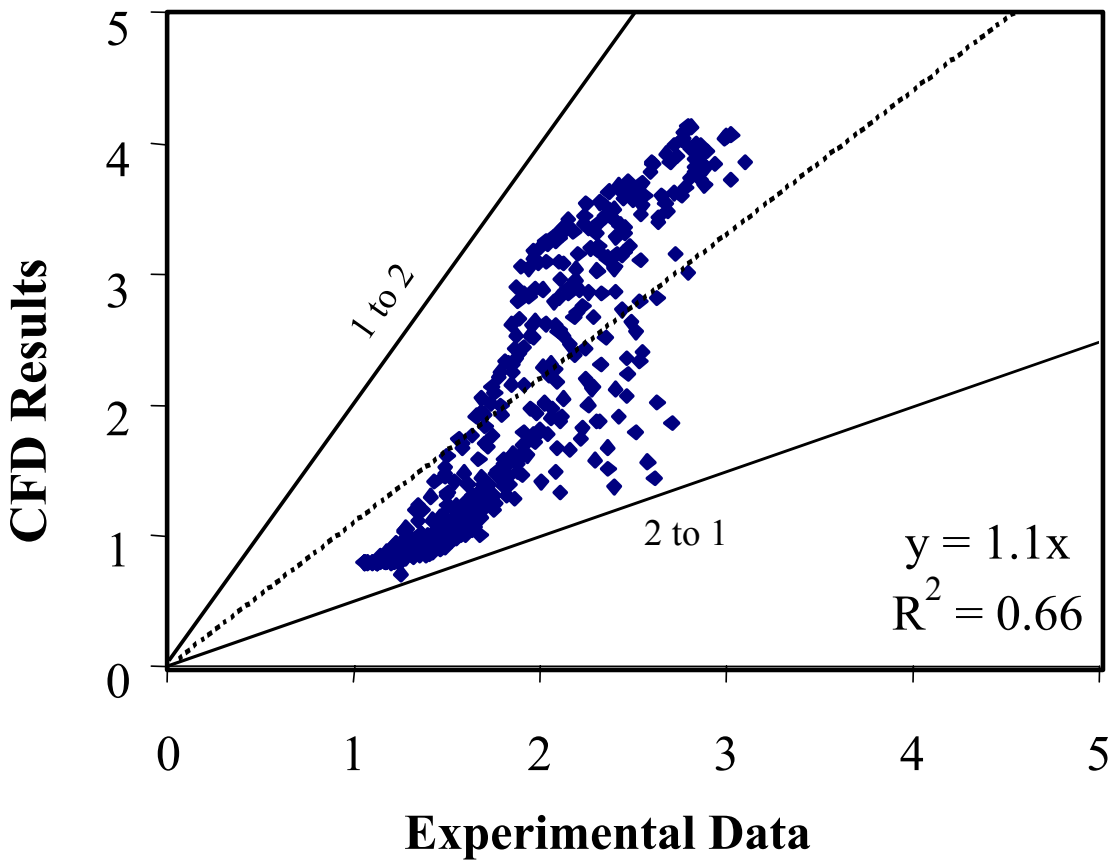

Figure 6. Comparison of the experimental data and the CFD results for the local concentration divided by the value of the fully mixed concentration in the experiment. The data points are average values from a grid with resolution of 1.3 x 1.3 cm, as described in the text. The linear regression formula is based on a fit that is forced to pass through the origin and is shown as a dotted line. The bounds of the factor-of-two agreement are show as solid lines.

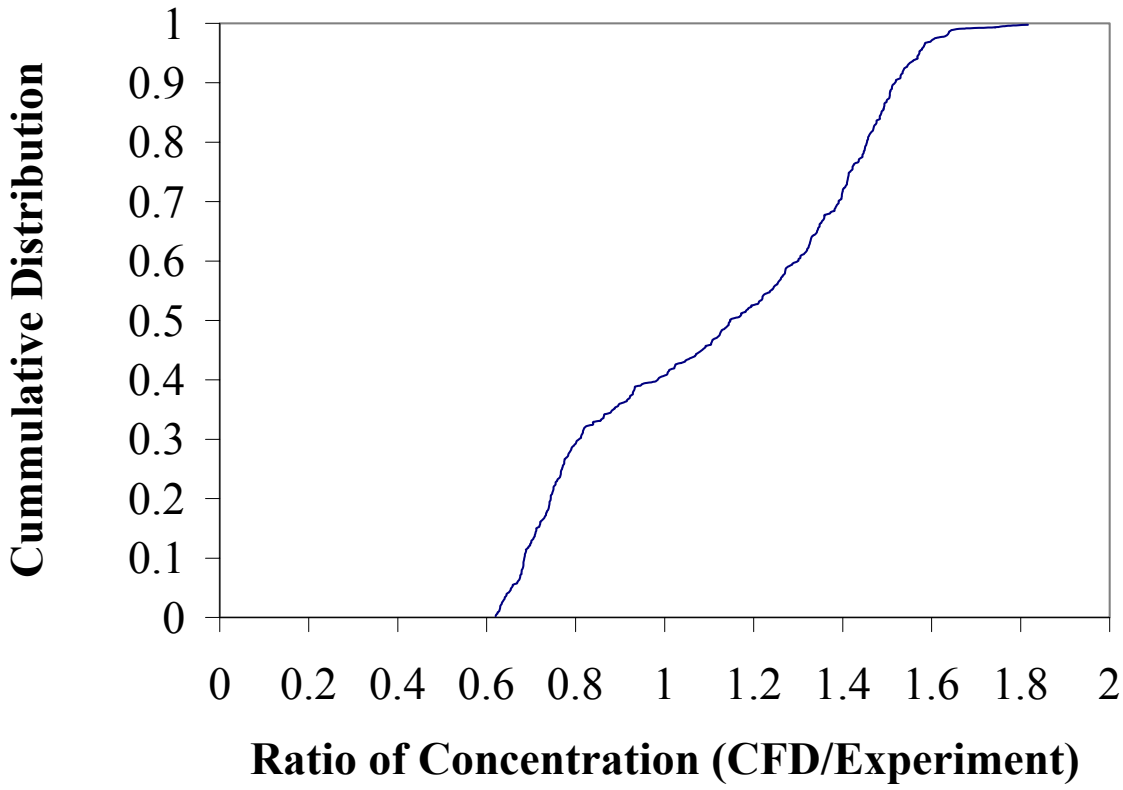

Figure 7 Cumulative distribution of the ratios of local concentrations (predicted vs. observed) in the measurement plane. The median value for the ratio is 1.15.

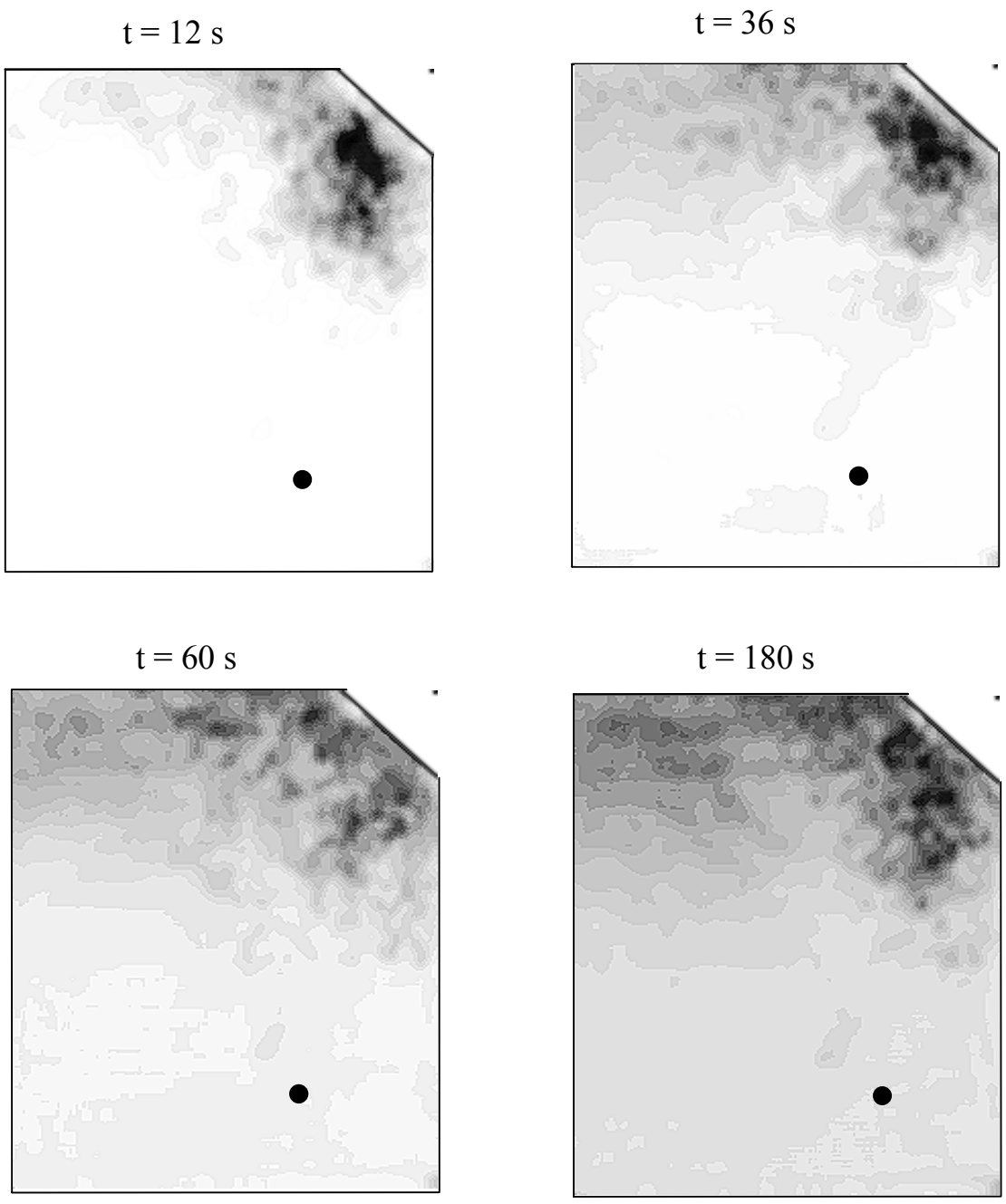

Figure 8: Dye concentrations in the measurement plane. The time is in seconds after initiation of dye release. The dye first appears in the measurement plane 5 seconds after the start of dye release. The flow in the tank is one tank volume per minute. The lower two images show the concentration after 1 and 3 volume changes. The black dot in each image indicates the location of the source, which was below the measurement plane.

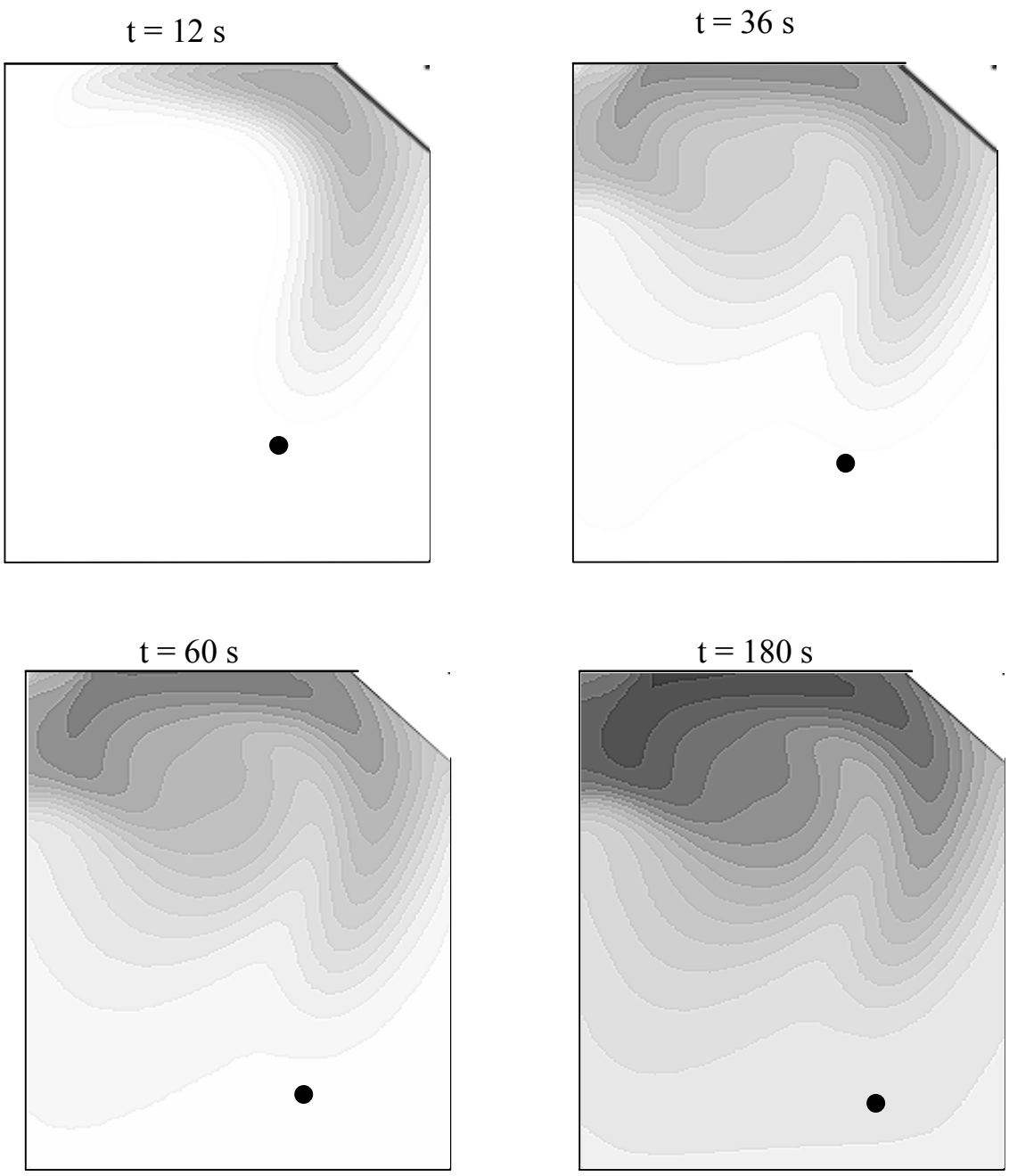

Figure 9: CFD simulation of dye concentrations in the measurement plane. The time is in seconds after initiation of dye release. The simulations show that the dye first appears in the measurement plane 4 seconds after the start of dye release. The flow in the tank is one tank volume per minute. The lower two images show the concentration after 1 and 3 volume changes. The black dot in each image indicates the location of the source, which was below the measurement plane.

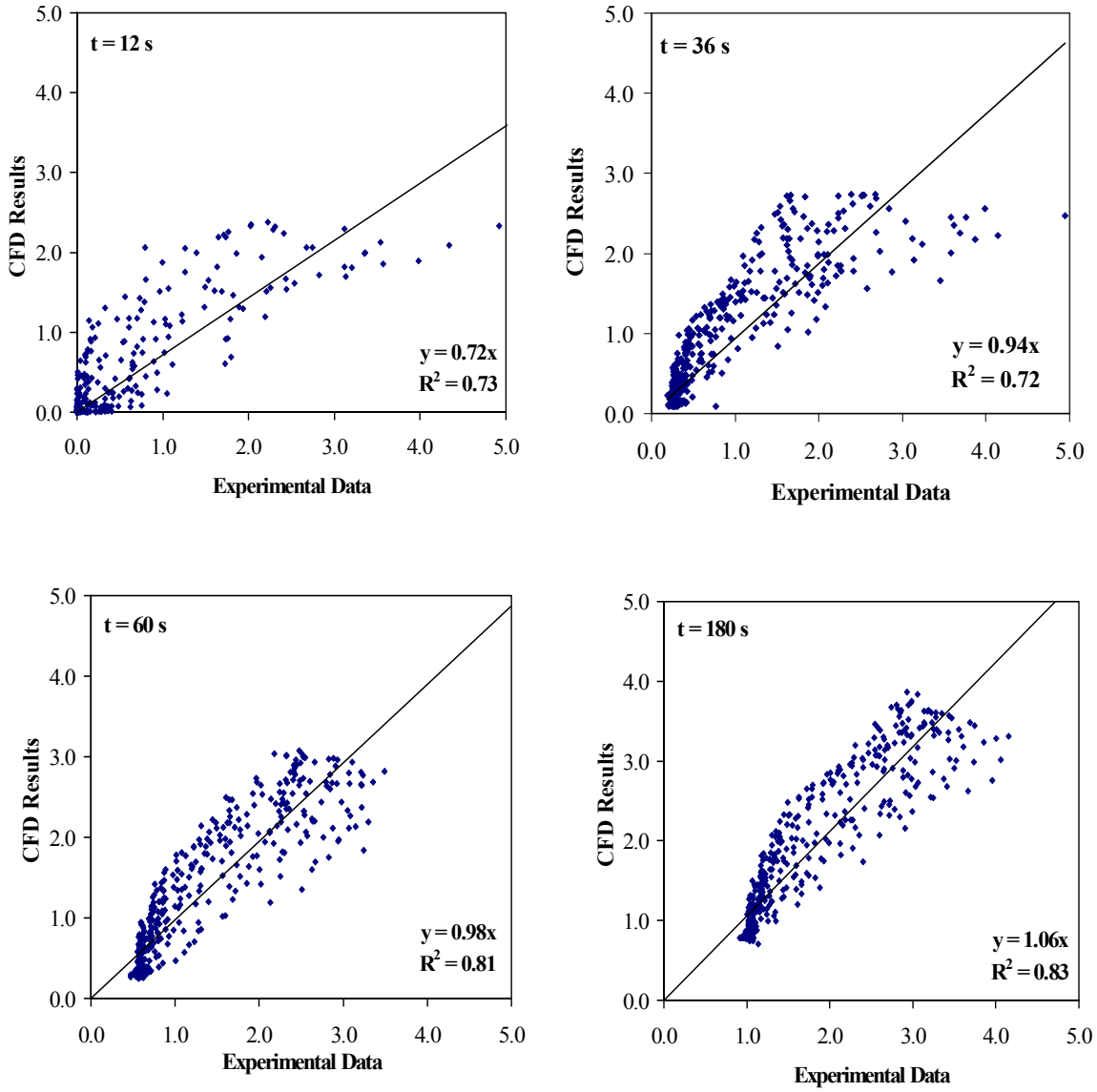

Figure 10. Quantitative comparison between the CFD results and the experimental data. The times shown correspond to those for the measured and predicted concentration contours shown in Figs. 8 and 9, respectively.

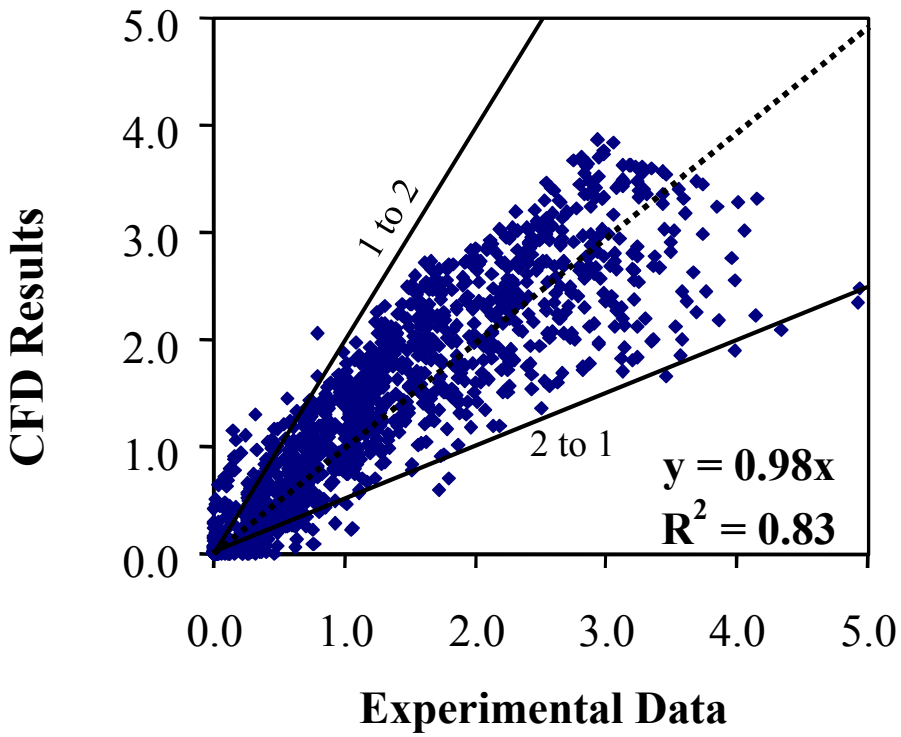

Figure 11 Comparison between experimental data and CFD predictions for the composite of the four times shown in Figure 10. The least square fit is shown as a dotted line. The bounds of the factor of 2 comparison are shown as solid lines. The factor of 2 criteria is well met except at very low concentrations. Due to the limited number of experiments used to obtain the developing averages concentration fluctuations can still be noticed in this data.